


Effect of Maintaining a Fixed Ambient Temperature on the Evaluation of Photovoltaic Device Performance

Ido Frenkel¹ and Avi Niv^{1*}

Swiss Institute for Dryland Environmental and Energy Research, Jacob Blaustein Institutes for Desert Research, Ben-Gurion University of the Negev, Sede Boqer Campus, 8499000, Israel

 (Received 7 January 2023; revised 4 April 2023; accepted 8 May 2023; published 7 June 2023)

In this article, we analyze the photovoltaic effect while assuming a fixed ambient temperature and a varying system temperature rather than using the standard fixed system temperature-based approaches. We do so by complementing the photon rate balance equation (detailed balance, circuit model) with the power balance equation of the system. As a result, a simple approach capable of treating any photovoltaic system emerges. Accordingly, we study the potential-dependent current and temperature of solar cells and thermoradiative power generators. We show that the optimal band gap of a solar cell depends on its heat-transfer coefficient and that its efficiency may rise or fall as solar concentration increases, depending on its ability to dissipate heat. We also identify where the cell's efficiency and temperature turn from a conductive and/or convective-dominated cooling regime to a radiative-dominated one. For the thermoradiative case, we show that its power decreases when heat intake is suppressed and study the degrading effect of nonradiative recombination on this power production scheme. The proposed model converges to the known fixed system temperature-based approaches when an infinite ability to transfer heat is considered.

DOI: [10.1103/PhysRevApplied.19.064023](https://doi.org/10.1103/PhysRevApplied.19.064023)

I. INTRODUCTION

In the photovoltaic (PV) effect, there is an intricate relation between the temperature at which it occurs, the electrical potential at which it is gauged, and the power it produces. Nonetheless, most theoretical analyses are carried out while considering a fixed PV system temperature, usually that of the ambient environment [1,2]. However, the excitation of electron-hole pairs generates entropy and thus produces heat. Therefore, a PV system must dissipate heat to accomplish steady-state conditions. Assuming a solar cell to be a lumped thermal system, i.e., of homogeneous temperature throughout each of the system's components, the cell can only dissipate heat if its temperature is higher than its ambient environment.

Previously, Dupre *et al.* [3,4] found the cell's steady-state temperature by meticulously formulating a closed-form expression for each possible heat-generating mechanism and balancing their sum with the heat transfer out of the cell. Expressing the heat generated at each step of the PV process is valuable for finding the performance-limiting mechanism of a given cell design. However, it is tailored for solar cells at standard conditions. Thus, it may become problematic under concentrated solar radiation, in outer space conditions, or in other situations where extreme conditions are encountered, such as thermal

PV [5,6], thermophotonic PV [7–9], and thermoradiative power generation schemes [10–12]. For thermoradiative and thermophotonic PVs, a power flux balance equation is an integral part of their analysis [10]. However, the role of heat transfer in the performance of these schemes has been overlooked. As a result, a unified approach that considers the net energy balance of a PV system, including heat transfer, is, thus far, lacking.

In this paper, we study the consequence of upholding the net power balance of a PV system, including heat transfer, in addition to the photon flux balance equation (the detailed balance). Since only the fundamental aspects of the PV effect are of interest, only ideal systems at their radiative limit are considered. Accordingly, optical confinement and optical absorption are neglected. Likewise, temperature-dependent changes in a material band gap or emissivity and a realistic model for the solar spectrum are ignored. Heat production is implicit in our model, so no assumptions are made about the nature of the heat-dissipating processes, resulting in a simpler formalism capable of treating any PV system.

We showcase our approach by examining a few types of PV systems. First, we study solar cells close to standard conditions. In this case, we verify that our formalism reproduces the expected potential-dependent current and temperature [3,4]. Nonetheless, appealing connections between the cell's ability to transfer heat and its temperature and open-circuit potential are discussed accordingly.

*aviniv@bgu.ac.il

We also study some example heat removal mechanisms and find that the efficiency of a single-junction cell may rise with solar concentration only if it has a sufficient ability to dissipate heat. Finally, we look at how thermoradiative power production is affected by the system's ability to drain heat from the hot environment it is in contact with, which is yet to be studied in this context.

II. POWER AND PHOTON RATE BALANCE EQUATIONS

Let us consider the photovoltaic system from Fig. 1: A PV system in the form of a cell receives radiation from the hot radiation source (sun) while emitting radiation to a colder environment (sky) due to radiative band-to-band recombination inherent in the PV process. The system also exchanges heat with its ambient environment, which can be conductive, convective, or radiative. Arrows indicate heat being carried away from the system, but this may change depending on the temperature difference between the system and its environment. Also, Fig. 1 depicts conductive, convective, and radiative (not band-to-band) heat transfer from the back of the cell for illustrative purposes only. In practice, these mechanisms are also active from the cell's sides and front face. In the following, we consider all these mechanisms, irrespective of their surface of origin. Finally, it is assumed that any property associated with the PV system, such as temperature or chemical potential, is uniform throughout its volume.

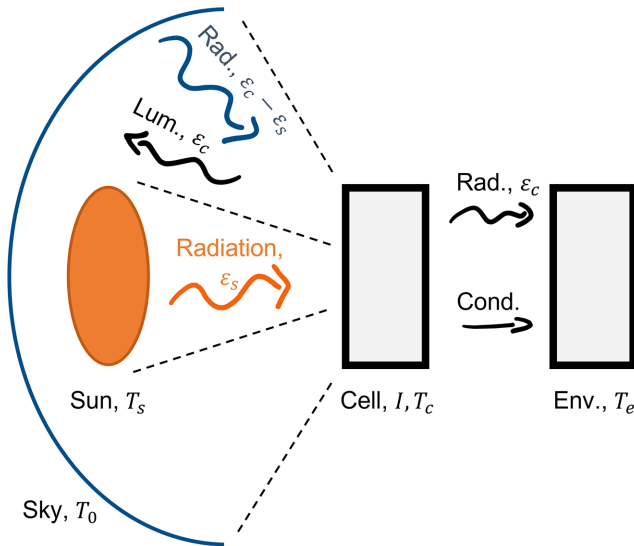


FIG. 1. The system under consideration comprises a cell that receives radiative heat from the sun and the sky at T_s and T_0 , respectively, and emits radiative heat and electron-hole band-to-band recombinations luminescence. The cell also rejects conductive and/or convective heat to the ambient environment at T_e .

The rate at which photons are received from the sun at a temperature T_s , is given by

$$\dot{N}_s = \frac{2\varepsilon_s}{c^2 h^3} \int_{E_g}^{\infty} \frac{E^2 dE}{\exp(E/kT_s) - 1}. \quad (1)$$

Here, c is the speed of light, h is Planck's constant, k is Boltzmann's constant. The PV process is considered ideal in the sense that it absorbs all light above the material band gap, E_g , and none below it. Formally, ε_s is the sun-to-cell etendue [13],

$$\varepsilon_s = \iint d\Omega dA, \quad (2)$$

with integration extending over the sun's solid angle and cell's area. For convenience, Eq. (2)'s spatial aspect would be suppressed such that a unitless reduced etendue (simply referred to as etendue henceforth) emerges, equivalent to a solid-angle view factor. Accordingly, the flux term of Eq. (1) and subsequent flux terms is per unit area. The system also receives photons from the portion of the sky not covered by the sun at the following rate:

$$\dot{N}_0 = \frac{2(\varepsilon_c - \varepsilon_s)}{c^2 h^3} \int_{E_g}^{\infty} \frac{E^2 dE}{\exp(E/kT_0) - 1}. \quad (3)$$

Here T_0 is the sky temperature ($T_0 < T_s$) and the cell's etendue is ε_c . Finally, photons are emitted due to the above-band-gap band-to-band recombination inherent in the PV process, the luminescence rate of which is

$$\dot{N}_c(T_c, V) = \frac{2\varepsilon_c}{c^2 h^3} \int_{E_g}^{\infty} \frac{E^2 dE}{\exp[(E - V)/kT_c] - 1}. \quad (4)$$

Here, V is the chemical potential of the PV process, henceforth to be referred to simply as potential. We also consider a flat system such that $\varepsilon_c = \pi$.

Assuming each absorbed photon excites one electron-hole pair, the current from the PV process is found by balancing the absorbed and emitted photon rates,

$$I/e = (\dot{N}_s + \dot{N}_0) - (\dot{N}_c + \dot{N}_{NR}), \quad (5)$$

where e is the fundamental charge and the nonradiative recombination rate, \dot{N}_{NR} , is a function of the system's temperature and potential. Equation (5) is the standard photon rate balance equation of Shockley and Queisser and others [1,2]. Equation (5) has the temperature, T , and the potential, V , as independent variables. Therefore, an additional constraint must be imposed to find the temperature and current at a given potential. We choose the energy exchange

rate of the system with its surroundings to perform this task,

$$VI/e = (\dot{U}_s + \dot{U}_0) - (\dot{U}_c + \dot{Q}). \quad (6)$$

On the left of Eq. (6) is the power generation term, and on the right side of Eq. (6), we have the power received from the sun, taken here as

$$\dot{U}_s = \frac{2\varepsilon_s}{c^2 h^3} \int_{E_g}^{\infty} \frac{E^3 dE}{\exp(E/kT_s) - 1}, \quad (7)$$

and from the rest of the sky as

$$\dot{U}_0 = \frac{2(\varepsilon_c - \varepsilon_s)}{c^2 h^3} \int_{E_g}^{\infty} \frac{E^3 dE}{\exp(E/kT_0) - 1}. \quad (8)$$

Equations (7) and (8) differ from the corresponding photon rates in Eqs. (1) and (3) by having an additional power of integration variable E . Like their corresponding rates for Eqs. (1) and (3), the source terms of Eqs. (7) and (8) are independent of the system temperature or potential and, therefore, along with Eqs. (1) and (3), can be replaced by alternative expressions for the photon flux and power from any known source, such as the AM1.5 solar spectrum.

Power leaving the system due to the above-band-gap PV radiative band-to-band recombination is given by

$$\dot{U}_c(T_c, V) = \frac{2\varepsilon_c}{c^2 h^3} \int_{E_g}^{\infty} \frac{E^3 dE}{\exp[(E - V)/kT_c] - 1}. \quad (9)$$

Here, T_c and V are the system's temperature and potential, whose values are the objective of the proposed approach. Finally, heat exchange between the system and its ambient environment at a temperature T_e is given by

$$\dot{Q} = h_c(T_c - T_e) + h_r \sigma (T_c^4 - T_e^4). \quad (10)$$

Two modes of heat transfer are considered in Eq. (10). The first is conduction or convection to an adjacent material, such as the surrounding air. This mechanism depends on the temperature difference between the cell and its ambient environment, and its magnitude is controlled with h_c , typical values of which are $10 - 20 \text{ Wm}^{-2} \text{ K}^{-1}$ [15,16], without differentiating between conduction or convection. The second type of heat transfer is radiative and thus proportional to the fourth power of the temperatures, i.e., $\propto(T_c^4 - T_e^4)$. The radiative cooling mechanism is additional to the band-to-band recombination mechanism from Eqs. (4) and (10) in transferring heat from the cell in the form of radiation, and may be active from any cell surface, back, sides, and front. This mechanism is controlled by a unitless relative emissivity from the surface of interest, h_r , and the parameter σ relating the electromagnetic energy

density that a surface emits to its temperature, which is obtained by suppressing the temperature dependency of Planck's law integrated over the relevant energy range,

$$\sigma = \frac{2\varepsilon_r k^4}{c^2 h^3} \int_a^b \frac{x^3 dx}{\exp(x) - 1}, \quad (11)$$

where ε_r is the view-factor unitless etendue of the radiative surface. The integration limits are $a = V_1 e k^{-1} T^{-1}$ and $b = V_2 e k^{-1} T^{-1}$, where $V_{1,2}$ defines the relevant energy range in electron volts. For example, if $V_1 = 0$, $V_2 = \infty$, and $\varepsilon_r = \pi$, then the Stefan-Boltzmann constant, $\sigma_{\text{SB}} = 5.67 \dots \times 10^{-5} \text{ Wm}^{-2} \text{ K}^{-4}$ emerges, whereas, $\sigma = 5.51 \times 10^{-11} \text{ Wm}^{-2} \text{ K}^{-4}$ is obtained for a 1000-K silicon slab ($V_1 = 0$, $V_2 = 1.12 \text{ eV}$). Notice that the combined radiative cooling from the different parts of a practical device, including sub-band-gap emission, can be introduced to Eq. (10) with a proper effective value of h_r and σ .

Equation (6) has the same form as Eq. (5) but considers the entire system, electron-hole population + lattice, instead of the electron-hole population alone, as Eq. (5) does. Being of the electron-hole population alone, Eq. (5) is deprived of any heat-to-lattice-related term (\dot{Q}). Complementary, the nonradiative recombination rate (\dot{N}_{NR}) does not remove power from the system, but only shifts it from the electron-hole population to the lattice and, therefore, is absent from Eq. (6). One may say that Eq. (5) includes processes that affect the potential, while Eq. (6) is for those that determine the temperature of the system. Equations (5) and (6) conserve the number of photons and the power they carry such that everything that enters the system must leave as current, radiation, or heat, and vice versa. Finally, it is easy to find by inspection that strict equilibrium is restored when it should be; for example, taking $I = 0$, $\varepsilon_s = \varepsilon_c$, and $h_c = 0$ gives $T_c = T_s$ and $V = 0$. In the following, we demonstrate the advantages of the proposed approach by numerically solving Eqs. (5) and (6) for different PV systems with different band gaps, heat conduction coefficients, solar concentrations, and nonradiative recombination rates.

III. POTENTIAL-DEPENDENT TEMPERATURE AND CURRENT

To find if our formalism can reproduce what can be considered known results for a solar cell [3,4], we calculate the potential-dependent current and temperature based on Eqs. (5) and (6) for a solar cell with band gap $E_g = 1 \text{ eV}$ in contact with an environment with $T_e = 300 \text{ K}$. Three values of the conduction/convection coefficient (h_c) are considered: high ($1000 \text{ Wm}^{-2} \text{ K}^{-1}$), intermediate ($20 \text{ Wm}^{-2} \text{ K}^{-1}$), and low ($5 \text{ Wm}^{-2} \text{ K}^{-1}$). The intermediate ("mid") case corresponds to what is considered typical for solar cells, while the low and the high values are two opposite extremes. In the following, the

exact amount of conduction or convection underlining the $\propto T$ processes in Eq. (10) is overlooked by assigning a single h_c , referred to as “conductivity” henceforth. Likewise, the role of the $\propto T^4$ radiative cooling is studied by nominating an effective $h_r\sigma$ product in Eq. (10), reflecting an arbitrary combination of thermal radiation from the cell’s front, back, or side facets and sub-band-gap emission from the PV material.

Figure 2(a) shows the resulting cell temperature as a function of its potential for these conductivity coefficients. In the low potential regime of 0–0.5 eV, the cell’s temperature can be approximated as $T_c = T_e - (e\dot{N}_s V - \dot{E}_s)/h_c$, as shown by the dashed black lines. As a result, the high conductivity case is practically at the ambient temperature (300 K), the low case reaches more than 200 K above the ambient at a short-circuit current (I for $V = 0$) and declines somewhat toward larger potentials, and the intermediate case sits between the other two. These relations allow one to find the effective conductivity coefficient from

the potential-dependent temperature of the cell. However, this requires prior knowledge of T_e , \dot{E}_s , and \dot{N}_s . In the following, we describe how the same result may be reached from the temperature dependence of the cell’s open-circuit potential (V at $I = 0$), which is often easier to measure. As the potential continues to increase, luminescence terms \dot{N}_c and \dot{E}_c in Eqs. (5) and (6) become appreciable, which further reduces the cell’s temperature. The temperature drop becomes significant above the open-circuit potentials (indicated with red asterisks) until it crosses the 300 K ambient temperature mark where the cell enters the light-emitting diode cooling regime [14].

Figure 2(b) shows the corresponding currents (solid lines, left axis) and powers (dashed lines, right axis) for the respective conductivities. Noticeable reduction in current and power emerges even for the intermediate case, corresponding to what is considered typical for a solar cell, and this is more noticeable for low conductivity. Short-circuit current (I at $V = 0$) shows only negligible dependence

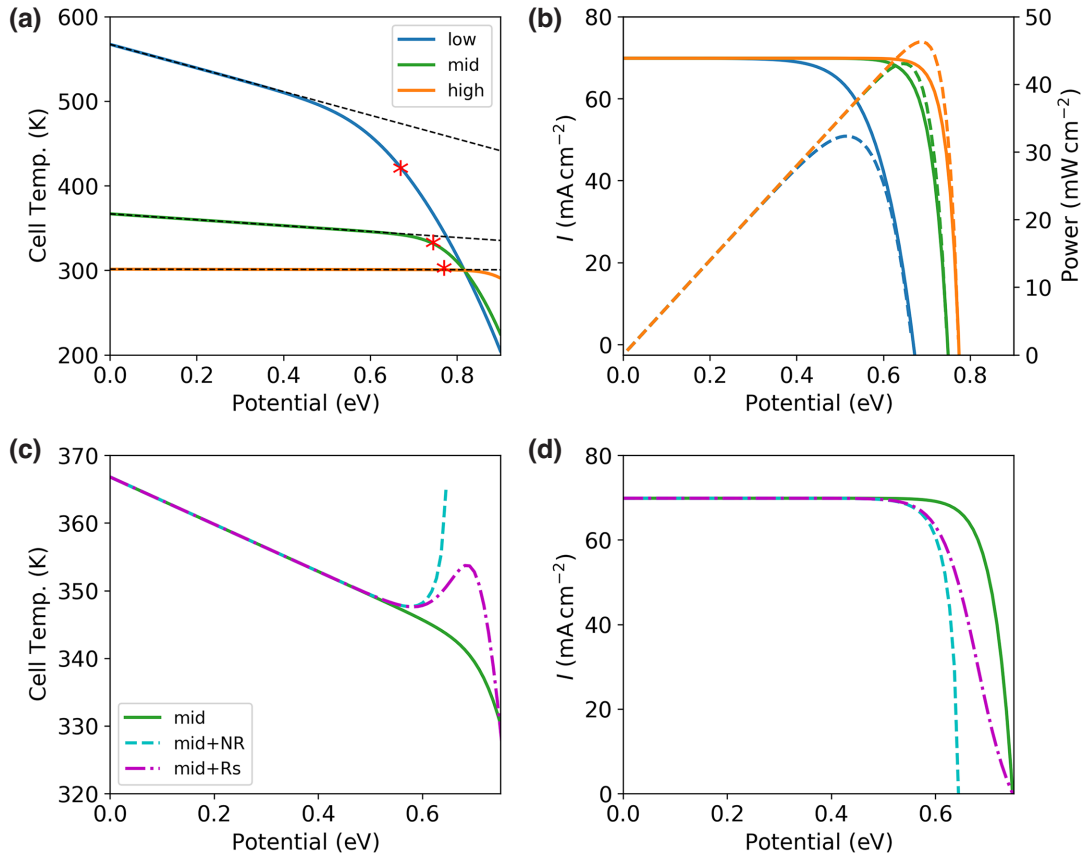


FIG. 2. (a) Potential-dependent cell temperature for low (blue, $h_c = 5 \text{ W m}^{-2} \text{ K}^{-1}$), medium (green, $h_c = 20 \text{ W m}^{-2} \text{ K}^{-1}$), and high (ocher, $h_c = 1000 \text{ W m}^{-2} \text{ K}^{-1}$) heat conduction coefficient (h_c). Red asterisks indicate the open-circuit voltage in each case. (b) Corresponding potential-dependent current (solid, left axis) and power (dashed, right axis). (c) Temperature profile for the pure intermediate heat conductivity case (solid green, $20 \text{ W m}^{-2} \text{ K}^{-1}$), the same heat conductivity but with nonideal radiative efficiency in a dashed cyan line labeled “mid + NR” ($\eta_R = 0.09$, $R_s = 0$), and the same heat conductivity but with series resistance only in a dashed-dotted magenta line labeled “mid + R_s ” ($R_s = 0.0001 \text{ } \Omega$, $\eta_R = 1$). (d) Corresponding currents. Notice the different x axis of (a),(b) relative to (c),(d). Other parameters: $T_s = 6000 \text{ K}$, $T_e = 300 \text{ K}$, $E_g = 1 \text{ eV}$, $\varepsilon_s = 6.87 \times 10^{-5}$, $\varepsilon_c = \pi$, $h_r = 0$.

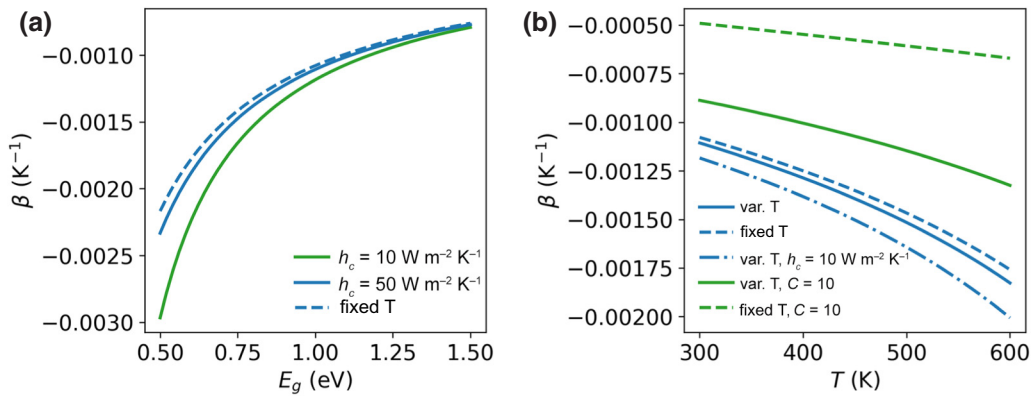


FIG. 3. (a) Open-circuit temperature sensitivity as a function of the band gap for heat conduction coefficient of 10 (green) and $50 \text{ Wm}^{-2} \text{ K}^{-1}$ (blue), respectively. The dashed blue line shows the corresponding fixed-temperature evaluation of this parameter at 300 K [15,16]. (b) Open-circuit temperature sensitivity as a function of the ambient temperature under the concentration of 1 (blue) and 10 (green) suns for heat conduction coefficient of $50 \text{ Wm}^{-2} \text{ K}^{-1}$. The corresponding fixed-cell-temperature (fixed T) evaluations of each case are shown in dashed lines. The dotted-dashed line shows a variable cell temperature evaluation under one sun with a heat conduction coefficient of 10 instead of $50 \text{ Wm}^{-2} \text{ K}^{-1}$.

on the conductivity value since the temperature-dependent band-gap narrowing is not considered here. Overall, Figs. 2(a) and 2(b) show our model's capability of reproducing what can be regarded as known results for a solar cell [3,4].

Series resistance, R_s , can be incorporated into our model by the usual variable exchange $V \rightarrow V + IR_s$. Also, a generic form of nonradiative combination is assumed by multiplying the $\dot{N}_c(T, V)$ term in Eq. (5) by $1/\eta_R$, where η_R is the radiative efficiency in this case. The radiative efficiency does not enter Eq. (6), since it only accounts for the internal redistribution between radiative and nonradiative processes, not the net power flux into or out of the PV system. Figure 2(c) shows the effect these nonidealities have on the potential-dependent temperature profile of the

intermediate heat conductivity case for $\eta_R = 0.09$ with $R_s = 0$ as a dashed cyan line, and for $R_s = 0.0001 \Omega$ and $\eta_R = 1$ as a dashed-dotted magenta line. Both nonidealities raise the cell's temperature close to its maximum power point potential in agreement with what has already been found, at least for the radiative efficiency [4]. Figure 2(d) shows the corresponding detrimental effect the rising cell temperature has on the cell's current in these cases. The $R_s \neq 0$ case demonstrates the ability of our approach to deal with Joule heating due to the fundamental series resistance of the PV material without an explicit term for such heat-generating processes in Eqs. (5) or (6). Other sources of Joule heating, like metal contacts, are not fundamental to the PV process and are, thus, neglected.

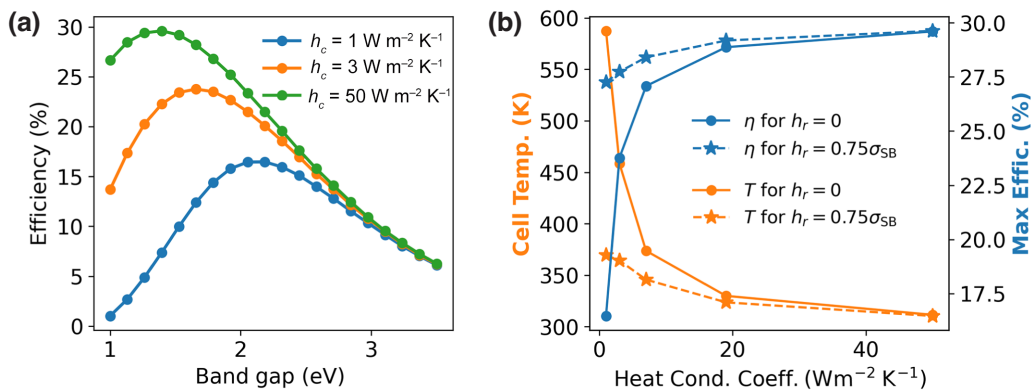


FIG. 4. (a) Band-gap-dependent cell efficiency for different heat conductivities (h_c) and no radiative cooling ($h_r = 0$). (b) Efficiency (blue) and temperature (ocher) at the band gap of maximal efficiency as a function of the heat conductivity is shown with circles. The results of an additional radiative cooling mechanism ($h_r \sigma = 0.75 \sigma_{\text{SB}}$) are marked with stars. Relevant parameters: $T_s = 6000 \text{ K}$, $T_e = 300 \text{ K}$, $T_0 = 4 \text{ K}$, $\epsilon_s = 6.87 \times 10^{-5}$, $\epsilon_c = \pi$, $\eta_R = 0.91$.

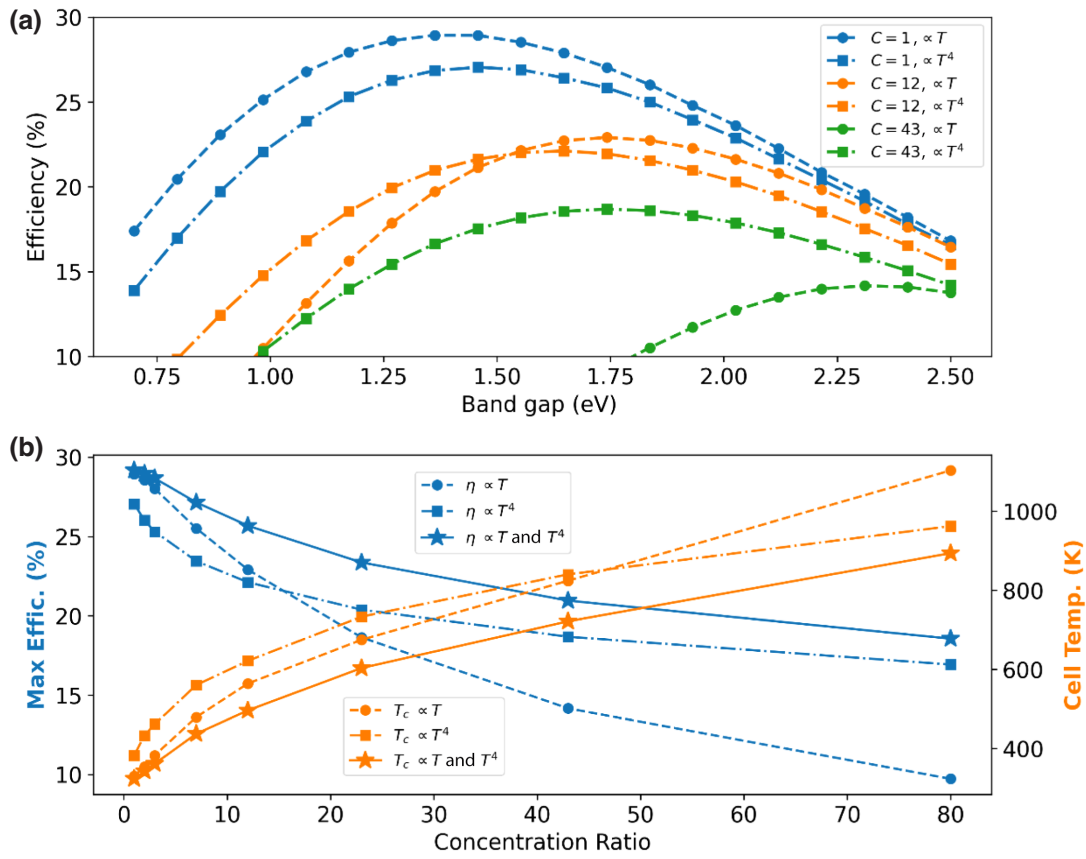


FIG. 5. (a) Band-gap-dependent efficiency for different solar concentrations (blue, $C = 1$; other, $C = 12$; green, $C = 43$). Two regimes are considered: heat conductivity only ($h_c = 20 \text{ W/m}^2 \text{ K}$, $h_r = 0$), and radiative cooling only ($h_c = 0$, $h_r = 0.75\sigma_{\text{SB}}$), which are marked with circles and squares, respectively. (b) Efficiency (blue, left y axis) and temperature (other, right y axis) at the maximal efficiency band gap as a function of the concentration ratio. Three cases are considered here: Two are the conductivity only and radiative only as in panel (a), respectively marked with circles and squares. In addition, a combined conductive-radiative regime is shown with stars. The conduction and radiation coefficients in (b) are identical to those in (a). Relevant parameters: $T_s = 6000 \text{ K}$, $T_e = 300 \text{ K}$, $T_0 = 4 \text{ K}$, $\varepsilon_s = 6.87 \times 10^{-5}$, $\varepsilon_c = \pi$, $\eta_R = 0.91$.

The open-circuit potential, V_{OC} , is another essential aspect of a solar cell's performance, the temperature coefficient of which is defined here as $\beta = d \ln(V_{\text{OC}})/dT = [dV_{\text{OC}}/dT]/V_{\text{OC}}$ [15,16]. Figure 3(a) shows, using a blue line, β as a function of the band gap E_g for an ideal cell (zero nonradiative recombination) with a heat conductivity coefficient of $50 \text{ Wm}^{-2} \text{ K}^{-1}$, and radiative cooling coefficient $h_r = 0$. The numerical derivative is calculated according to the following finite-difference formula: $dV_{\text{OC}}(T_e)/dx = [V_{\text{OC}}(T_e + \Delta T_e) - V_{\text{OC}}(T_e - \Delta T_e)]/2\Delta T_e$. Convergence is achieved for $\Delta T_e < 10 \text{ K}$ at a nominal $T_e = 300 \text{ K}$. The β parameter's dependence on the system's ability to dissipate heat is shown with the green line of Fig. 3(a) for a heat conductivity of $10 \text{ Wm}^{-2} \text{ K}^{-1}$. The more negative the value of β is, the larger the reduction in V_{OC} once the ambient temperature rises. The larger absolute value of the β factor at smaller band gaps comes from a more significant thermalization-driven heat source within the cell. For comparison, we also show the result of a fixed cell

temperature-based evaluation of β , following Ref. [15] (with the free parameter $\gamma = 2$), which is oblivious to the system's heat conductivity.

Figure 3(b) shows β as a function of the ambient temperature for a 1-eV-band-gap ideal radiative cell with heat conductivity of $50 \text{ Wm}^{-2} \text{ K}^{-1}$ as a solid blue line (h_r is still held at its zero value). It is seen that the fixed system (cell) temperature-based evaluation, shown with a dashed blue line, undermines the degrading effect that temperature has on V_{OC} relative to our ambient temperature-based approach. The difference between a cell-based and an ambient-based approach becomes more pronounced for the same cell but with a 10-sun concentration, as seen in the green solid and dashed lines. Finally, we show with a dashed-dotted blue line the value of β for the same ideal 1-eV cell but with a reduced heat conductivity of $10 \text{ Wm}^{-2} \text{ K}^{-1}$. Once again, there is no correspondence to this effect in the fixed cell temperature-based evaluation approach. The different trend that emerges, in this case, points to the possibility of

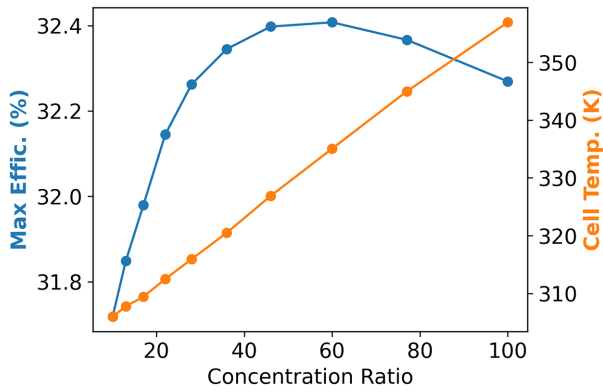


FIG. 6. Efficiency and temperature at optimal 1.29-eV band gap as a function of the solar concentration ratio for heat conduction coefficient $h_c = 1000 \text{ Wm}^{-2} \text{ K}^{-1}$. Relevant parameters: $T_s = 6000 \text{ K}$, $T_e = 300 \text{ K}$, $T_0 = 4 \text{ K}$, $\varepsilon_s = 6.87 \times 10^{-5} \text{ m}^2$, $\varepsilon_c = \pi$, $\eta_R = 0.91$.

identifying the effective heat conductivity of a PV system based on the measured temperature coefficient of its V_{OC} .

IV. BAND-GAP-DEPENDENT EFFICIENCY AND TEMPERATURE

Next, let us study how a cell's ability to dissipate heat affects temperature and its efficiency, which is $\eta = \max(VI)/P_s$, with $P_s = (\varepsilon_s/\pi)\sigma T_s^4$ the total incoming power, which is 1607 Wm^{-2} for the 6000 K black body considered here as the sun. Figure 4(a) shows the band-gap-dependent efficiency for selected heat conductivity values (and no radiative cooling). It is seen that lower conductivity reduces the efficiency while shifting the maximal efficiency to higher band gaps, in agreement with previous studies [3,4]. This effect is because smaller band gaps result in more thermalization, which causes the efficiency to be more sensitive to the conductivity coefficient value.

Suppressing heat dissipation causes the cell's temperature to rise and its maximal efficiency to decrease, as seen in Fig. 4(b). At 29.6%, the efficiency at $h_c = 50 \text{ Wm}^{-2} \text{ K}^{-1}$ without radiative cooling is close to the 30% of a fixed-cell-temperature evaluation, and the cell is less than 1 K above its 300 K ambient temperature. Once the conductivity coefficient is lower than $20 \text{ Wm}^{-2} \text{ K}^{-1}$, the cell's temperature rises sharply, and the maximal efficiency decreases, which is interesting since the heat-transfer coefficient of practical modules is expected to lie in this range, i.e., the $10 - 20 \text{ Wm}^{-2} \text{ K}^{-1}$ range [4].

As the cell's temperature rises, radiative cooling is expected to play a more decisive role due to its $\propto T^4$ dependence. To see how this effect comes about, we consider the case where, in addition to the varying heat conductivity value in Fig. 4(b), there is also a radiative cooling with an effective $h_r\sigma = 0.75\sigma_{SB}$ (σ_{SB} is the Stefan-Boltzmann

constant). This effective value considers all $\propto T^4$ radiative transfer mechanisms without differentiating their exact source, be it sub-band-gap emission of the PV material or thermal radiation from other parts of the cell. It is seen that the addition of radiative cooling significantly reduces the cell's temperature when its ability to conduct heat is low, resulting in higher efficiencies at low conductivities. However, as the conductivity increases above $20 \text{ Wm}^{-2} \text{ K}^{-1}$, the cell's temperature lowers and is no longer affected by radiative cooling. In the following, we further study the crossover between these two heat-transfer regimes, but this time under concentrated solar radiation, where heat dissipation plays a more crucial role in the cell's performance.

V. CELL PERFORMANCE UNDER CONCENTRATED SOLAR RADIATION

A more convincing demonstration of allowing the cell's temperature to adjust its environment emerges for concentrated solar radiation. Figure 5(a) shows the efficiency for solar concentrations of $C = 1$ in blue, $C = 12$ in ochre, and $C = 43$ in green. In addition, two heat-transfer regimes are considered: the first focuses on the $\propto T$ convection and conduction by taking $h_c = 20 \text{ Wm}^{-2} \text{ K}^{-1}$ and $h_r\sigma = 0$, which is marked with circles, while the second is for the $\propto T^4$ sub-band-gap and thermal radiation processes with $h_c = 0$ and $h_r\sigma = 0.75\sigma_{SB}$, which is marked with squares. Dramatic reduction in efficiency is seen with rising concentration for both cases. Interestingly, the optimal band gap shifts to higher values as the concentration rises, which is opposite to what is found from a fixed cell temperature-based evaluation [17].

To better understand this behavior, we plot in Fig. 5(b) the maximal band-gap-dependent efficiency in blue and the cell's temperature in ochre. The efficiencies and temperatures are plotted as a function of the concentration for the former $\propto T$ and $\propto T^4$ heat-transfer regimes, and are marked with the same circles and squares, respectively. The advantage of the $\propto T$ regime at low concentrations and that of the $\propto T^4$ at higher concentration repeat here. Interestingly, the crossover between these two regimes does not occur at the same concentration levels for the efficiency and the cell's temperature. While the efficiency of the radiative $\propto T^4$ case already surpasses that of the $\propto T$ case by $C > 12$, it is not until $C > 43$ that the cell's temperature from the radiative $\propto T^4$ processes falls below that of the conductive $\propto T$ case. Going back to Fig. 5(a), we see that the maximal efficiency in the $\propto T$ regime is better at lower concentrations while the opposite is true for the higher ones, which is the source of the efficiency crossover in Fig. 5(b) at a little over $C = 12$. The tendency of maximal efficiency to appear at larger band gaps as concentration rises reduces the cell's temperature by suppressing thermalization, thus delaying the temperature crossover between the two regimes. The

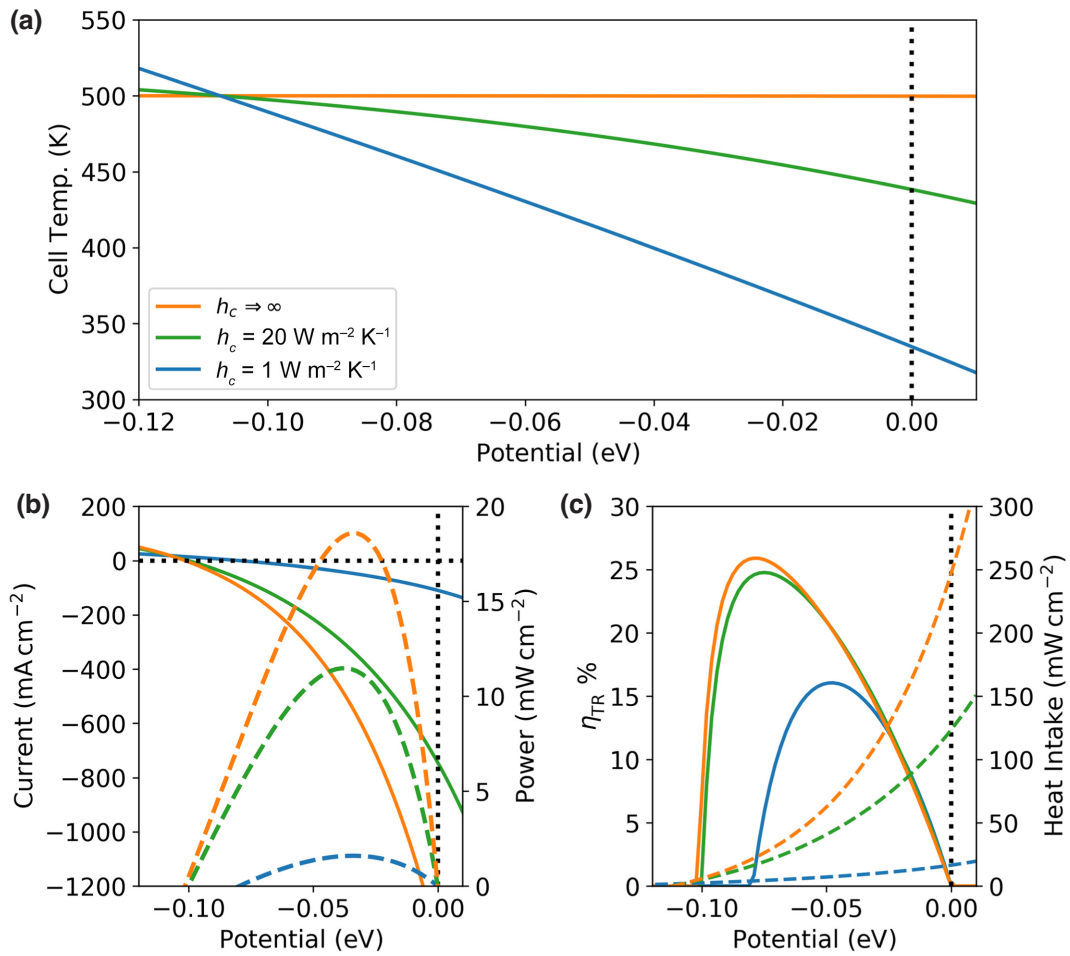


FIG. 7. (a) Thermoradiative cell’s temperature for different heat conductivities. The $h_c \Rightarrow \infty$ case corresponds to a fixed-cell-temperature evaluation. (b) The current (left y axis) and power (right y axis) of the different heat conductivities are shown in solid and dashed lines, respectively. (c) The corresponding efficiency (left y axis) and heat intake (right y axis) are in solid and dashed lines, respectively. Relevant parameters: $T_e = 500 \text{ K}$, $T_0 = 300 \text{ K}$, $\varepsilon_s = 0$, $\varepsilon_c = \pi$, $\eta_R = 1$, $h_r = 0$.

results in Fig. 5(b) are presented for a changing optimal band gap, according to Fig. 5(a).

Practical cells are expected to benefit from both these mechanisms, as shown by the stars in Fig. 5(b). As expected, the combination produces better efficiency and lower temperatures than each independent regime and tends to the conductive case at lower concentrations while converging to the radiative regime at higher ones. It is important to note that while separate efficiency and temperature crossovers are generic features, their exact positions are prone to specific device parameters. Therefore, the values reported here should be considered for demonstration purposes only and not for a practical cell design.

Another interesting point is that the cell’s efficiency in our ambient-centric approach decreases at higher concentrations, unlike in a cell-centered one [17]. To see why this seemingly contradictory behavior emerges, Fig. 6 shows the maximal efficiency and cell temperature for the

same cell as in Fig. 5, but with a much larger heat conductivity of $1000 \text{ W m}^{-2} \text{ K}^{-1}$ ($h_r = 0$, in this case). It is seen that a rise in efficiency as concentration increases may be restored, at least for concentration ratios smaller than 50 in this case. Interestingly, the cell’s temperature scales linearly with concentration, in this case, and the optimal band gap is fixed at 1.29 eV. It should be noted that such an ability to dissipate heat is only expected to be found in microcells due to their high surface-to-volume ratio [18]. Alternatively, multijunction cells may demonstrate such an increase in efficiency due to their reduced thermalization losses [19,20].

VI. THERMORADIATIVE POWER GENERATION

Thermoradiative power generation is the opposite of a solar cell: power is produced by absorbing conductive heat from a hot source and radiating to a colder environment. As such, heat intake is integral to the theoretical analysis

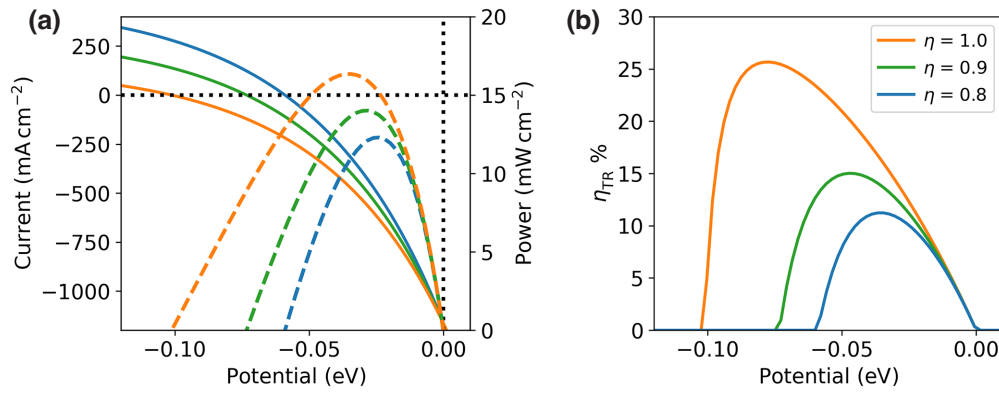


FIG. 8. (a) Thermoradiative current versus cell potential for different nonradiative (NR) recombination rate coefficients (solid lines, left y axis) and the corresponding power (dashed, right y axis). (b) The related efficiencies of each case. Other parameters: $T_e = 500$ K, $T_0 = 300$ K, $\varepsilon_s = 0$, $\varepsilon_c = \pi$, $h_c = 100$ W m⁻² K⁻¹.

of thermoradiative PVs [10–12]. Surprisingly, the effect of finite heat conduction has so far been overlooked. To demonstrate the ability of our formalism to tackle this situation and provide insight into the role of less-than-ideal heat conduction, we solve for the potential-dependent current and temperature of a 0.1-eV-band-gap cell in contact with a hot environment, $T_e = 500$ K, with no sun ($\varepsilon_s = 0$), that radiates its band-to-band emission to a cold environment, $T_0 = 300$ K. Notice that Eqs. (5) and (6) are indifferent to whether a solar or a thermoradiative cell is considered.

Figure 7(a) shows the thermoradiative cell’s temperature as a function of the potential for different heat conduction coefficients. Infinite heat conductivity converges to a fixed-cell-temperature evaluation, where the cell and the environment temperature are identical [10]. All temperature curves cross the hot environment at 500 K independently of the cell’s heat conductance. This effect is caused by having $\dot{Q} = 0$ in Eq. (6), in this case, resulting in current and temperature values being independent of the heat conductivity value. Radiative cooling other than band-to-band recombination is overlooked to allow a meaningful comparison with former results [10]. In addition, radiative cooling is expected to play a minor role in the $T_c < 500$ K range of interest. Figure 7(b) shows with solid lines (left axis) and dashed lines (right axis) the corresponding currents and powers, respectively. Negative currents result from the cell being hotter than the environment it radiates to (negative illumination). The respective power, VI , is positive since both potential and current are negative in the power production quadrant delineated by the dotted black lines of Fig. 7(b). The currents coalesce at a positive value outside the power production quadrant corresponding to the heat conductivity-independent point of the temperatures.

Figure 7(c) shows the thermoradiative efficiency—the output power divided by heat absorbed from the hot

environment [10–12],

$$\eta_{\text{TR}} = \frac{VI}{|\dot{Q}|}. \quad (12)$$

It is seen that the infinite conductivity case peaks at a little over 25%, in agreement with the fixed-system-temperature evaluation of this case [10], while the lower conductivity cases are below 25% and a little over 15% for the 20 and 1 W m⁻² K⁻¹ conductivities, respectively. Maximal power point and maximal efficiency potentials are not the same, as seen by comparing the dashed lines of Fig. 7(b) with the solid ones of Fig. 7(c). This difference emerges from the more considerable gap that emerges between the system and the ambient temperatures as the potential decreases in its absolute value, as seen in Fig. 7(a), and the corresponding larger heat intake, $|\dot{Q}|$, that develops as a result, and is shown by the dashed lines in Fig. 7(c).

Nonradiative recombination poses a significant limitation on the ability of thermoradiative power generation. Figure 8 shows the same thermoradiative cell as in Fig. 7, but this time with a fixed 100 W m⁻² K⁻¹ heat conductivity and different amounts of nonradiative recombination expressed as different values of the radiative efficiency η_R . The apparent smaller current, power, and efficiency that emerge for a smaller radiative efficiency, η_R , demonstrate our approach’s ability to account for the detrimental effect that nonradiative recombination has on the performance of thermoradiative PVs in much the same way as is done for solar cells.

VII. SUMMARY AND CONCLUSIONS

This work concerns the consequences of shifting the theoretical PV analysis from considering a fixed system temperature to a fixed ambient temperature and the ensuing heat transfer in the form of conduction, convection, and

radiation. To do so, we find the temperature and electrical potential that mutually solve the PV photon rate and power balance equations. The photon balance is for the electron-hole pair population only (detailed balance), while the power balance is the net power absorbed or released by the system.

We show that, according to the proposed approach, the maximal efficiency of a solar cell decreases and shifts to larger band gaps relative to a fixed-cell-temperature evaluation, as its ability to dissipate heat is suppressed, in agreement with previous studies. We also point to the connection between the heat-transfer coefficient of a cell, its temperature, and the temperature coefficient of its open-circuit voltage. We identify separate efficiency and cell temperature crossovers from a conductive- or convective-dominated regime to a radiative-dominated one as a function of the solar concentration. We also find an efficiency drop at moderate concentrations for a typical heat conductivity of single-junction solar cells, which is opposite to the result from a cell-oriented evaluation. The expected efficiency rise is restored once an exceptional ability to transfer heat is considered.

Finally, we study PV power production by negative illumination—the thermoradiative approach. There we find good agreement with known models of an ideal cell and demonstrate our approach’s ability to tackle nonradiative recombination and the yet-to-be-accounted-for less-than-infinite heat conductivity.

In conclusion, we show that considering the cell temperature as a function of the external parameters, including the heat-transfer coefficients, for a fixed ambient temperature may lead to different and even opposite predictions relative to the fixed system temperature–based approach. We believe that a fixed ambient temperature–based evaluation better represents the actual operating conditions of PV systems. Alas, this work considers the PV effect in its fundamental form. Accordingly, other phenomena affecting the performance of a PV device, like optical confinement and finite absorption, are neglected. Likewise, a temperature-dependent band gap, a more realistic solar spectrum, and the exact form of various nonradiative recombination mechanisms (Shockley-Read-Hall, Auger) are ignored. A more realistic evaluation of a specific PV device can be obtained by readily incorporating these effects into our model.

The code used in this work would be made available upon a reasonable request from the corresponding author (A. Niv).

ACKNOWLEDGMENTS

We extend our gratitude to Professor Visoly-Fisher and Professor Eugene Katz for their helpful comments regarding the preparation of this manuscript.

I.F. and A.N. formulated the model, performed the analysis, and wrote the manuscript. A.N. conceptualized and supervised the project.

The author(s) declare no competing interests.

-
- [1] J. F. Guillemoles, T. Kirchartz, D. Cahen, and U. Rau, Guide for the perplexed to the Shockley–Queisser model for solar cells, *Nat. Photonics* **13**, 501 (2019).
 - [2] W. Shockley and H. J. Queisser, Detailed balance limit of efficiency of p-n junction solar cells, *J. Appl. Phys.* **32**, 510 (1961).
 - [3] O. Dupre, R. Vaillon, and M. A. Green, A full thermal model for photovoltaic devices, *Sol. Energy* **140**, 73 (2016).
 - [4] O. Dupre, R. Vaillon, and M. A. Green, *Thermal Behavior of Photovoltaic Devices* (Springer, 2017).
 - [5] Z. Zhou, E. Sakr, Y. Sun, and P. Bermel, Solar thermophotovoltaics: Reshaping the solar spectrum, *Nanophotonics* **5**, 1 (2016).
 - [6] A. Licht, N. Pfiester, D. Demeo, J. Chivers, and T. E. Vanderveelde, A review of advances in thermophotovoltaics for power generation and waste heat harvesting, *MRS Adv.* **4**, 2271 (2019).
 - [7] N. Harder and M. A. Green, Thermophotonics, *Semicond. Sci. Technol.* **18**, S270 (2003).
 - [8] T. Sadi, I. Radevici, and J. Oksanen, Thermophotonic cooling with light-emitting diodes, *Nat. Photonics* **14**, 205 (2020).
 - [9] T. Sadi, I. Radevici, B. Behaghel, and J. Oksanen, Prospects and requirements for thermophotonic waste heat energy harvesting, *Sol. Energy Mater. Sol. Cells* **239**, 111635 (2022).
 - [10] R. Strandberg, Theoretical efficiency limits for thermoradiative energy conversion, *J. Appl. Phys.* **117**, 055105 (2015).
 - [11] T. Liao, Z. Yang, X. Chen, and J. Chen, Thermoradiative-photovoltaic cells, *IEEE Trans. Electron Devices* **66**, 386 (2019).
 - [12] W.-C. Hsu, J. K. Tong, B. Liao, Y. Huang, S. v. Boriskina, and G. Chen, Entropic and near-field improvements of thermoradiative cells, *Sci. Rep.* **6**, 34837 (2016).
 - [13] T. Markvart, The thermodynamics of optical etendue, *J. Opt. A: Pure Appl. Opt.* **10**, 015008 (2007).
 - [14] T. P. Xiao, K. Chen, P. Santhanam, S. Fan, and E. Yablonovitch, Electroluminescent refrigeration by ultra-efficient GaAs light-emitting diodes, *J. Appl. Phys.* **123**, 173104 (2018).
 - [15] O. Dupre, R. Vaillon, and M. A. Green, Physics of the temperature coefficients of solar cells, *Sol. Energy Mater. Sol. Cells* **140**, 92 (2015).
 - [16] A. Braun, E. A. Katz, and J. M. Gordon, Basic aspects of the temperature coefficients of concentrator solar cell performance parameters, *Prog. Photovoltaics* **21**, 1087 (2013).
 - [17] J. Zeitouny, N. Lalau, J. M. Gordon, E. Katz, G. Flamant, A. Dollet, and A. Vossier, Assessing high-temperature photovoltaic performance for solar hybrid power plants, *Sol. Energy Mater. Sol. Cells* **182**, 61 (2018).
 - [18] M. Paire, L. Lombez, N. Pere-Laperne, S. Collin, J. Pelouard, D. Lincot, and J. Guillemoles, Microscale

- solar cells for high concentration on polycrystalline Cu(In,Ge)Se₂ thin films, [Appl. Phys. Lett.](#) **98**, 264102 (2011).
- [19] H. Cotal, C. Fetzer, J. Boisvert, G. Kinsey, R. King, P. Herbert, H. Yoon, and N. Karam, III-V multijunction solar cells for concentrating photovoltaics, [Energy Environ. Sci.](#) **2**, 174 (2009).
- [20] S. Kurtz and J. Geisz, Multijunction solar cells for conversion of concentrated sunlight to electricity, [Opt. Express](#) **18**, A73 (2010).